Hydrothermal Carbonization of Various Paper Mill Sludges: An Observation of Solid Fuel Properties

Nepu Saha [1,2] [ID], **Akbar Saba** [1,3], **Pretom Saha** [1,3], **Kyle McGaughy** [1,2],
Diana Franqui-Villanueva [4], **William J. Orts** [4], **William M. Hart-Cooper** [4] and
M. Toufiq Reza [1,2,*] [ID]

[1] Institute for Sustainable Energy and the Environment, Ohio University, Athens, OH 45701, USA;
ns671517@ohio.edu (N.S.); as030616@ohio.edu (A.S.); ps332316@ohio.edu (P.S.); km067812@ohio.edu (K.M.)

[2] Department of Chemical and Biomolecular Engineering, Ohio University, Athens, OH 45701, USA

[3] Department of Mechanical Engineering, Ohio University, Athens, OH 45701, USA

[4] USDA-PWA, ARS, WRRC, BCE, 800 Buchanan Street, Albany, CA 94710, USA;
diana.franqui@ars.usda.gov (D.F.-V.); bill.orts@ars.usda.gov (W.J.O.);
william.hart-cooper@ars.usda.gov (W.M.H.-C.)

[*] Correspondence: reza@ohio.edu; Tel.: +1-740-593-1506

Abstract: Each year the pulp and paper industries generate enormous amounts of effluent treatment sludge. The sludge is made up of various fractions including primary, secondary, deinked, fiber rejects sludge, etc. The goal of this study was to evaluate the fuel properties of the hydrochars produced from various types of paper mill sludges (PMS) at 180 °C, 220 °C, and 260 °C. The hydrochars, as well as the raw feedstocks, were characterized by means of ultimate analysis, proximate analysis, moisture, ash, lignin, sugar, and higher heating value (HHV$_{daf}$) measurements. Finally, combustion indices of selected hydrochars were evaluated and compared with bituminous coal. The results showed that HHV$_{daf}$ of hydrochar produced at 260 °C varied between 11.4 MJ/kg and 31.5 MJ/kg depending on the feedstock. This implies that the fuel application of hydrochar produced from PMS depends on the quality of feedstocks rather than the hydrothermal carbonization (HTC) temperature. The combustion indices also showed that when hydrochars are co-combusted with coal, they have similar combustion indices to that of coal alone. However, based on the energy and ash contents in the produced hydrochars, Primary and Secondary Sludge (PPS$_2$) could be a viable option for co-combustion with coal in an existing coal-fired power plant.

Keywords: primary sludge; secondary sludge; deinked sludge; fiber rejects; hydrochar; combustion indices; fuel properties

1. Introduction

The world energy demand continues to grow with the increase of populations. The energy demand is projected to reach up to 42 quadrillion British Thermal Unit (BTU) in 2040 to fulfill the needs of 10 billion people [1,2]. In order to ensure this energy supply is provided in a sustainable manner, fossil fuel industries need to begin integrating with renewable energy sources. Coal power plants, one of the major electricity producers in the U.S., are still expected to provide 17.6% more electricity in 2040 compared to today [2]. This sustainability problem provides extraordinary potential for coal-like fuels generated from renewable resources. Wet waste biomass, such as paper mill sludges (PMS), is one of the largest and most abundant sources of renewable energy [3]. In fact, around 16.5 million dry tons of PMS have been produced annually in the U.S. These wastes have been landfilled, land applied, incinerated, or used in other ways (e.g., filler, fibers, composite etc.) [4]. Due to the strict landfill

policies and shortage of lands, incineration is becoming the preferred treatment method despite having incineration costs of around $13–15 per dry ton [5]. Co-firing PMS with coal in existing coal-fired power plants may reduce the carbon footprint for the power plant and it may reduce the cost of waste disposal for the paper mill by generating a sellable product rather than waste [6,7]. However, viable co-firing requires a feedstock of consistent quality with higher energy density and combustion characteristics compatible with coal.

A wide variety of PMS are generated in the pulp and paper mills [8–10]. PMS can be categorized into four broad sections: (1) primary sludge (PS), which is produced in the primary clarifier and contains mainly fines and fillers [11]; (2) de-inking paper sludge (DPS), which is produced during the floatation process and is very common for recycled papers [12]; (3) secondary sludge (SS) or biological sludge, which is the effluent of the microbial wastewater treatment system and is made of microbial masses [10]; and (4) combined primary and secondary sludge (PSS), which is a mixture of primary and secondary sludges from the same plant [13]. Besides these basic four categories, there could be preliminary fiber rejects (PFR) containing preliminary impurities such as metals, inorganics, plastics, tree branches, etc. and pre-thickened sludge (PTS), which is primary sludge prior to the dewatering step [14]. The chemical composition of the PMS varies significantly among these categories [8]. For instance, PS is more fibrous and easier to dewater when compared to SS and PSS [11]. DPS contains pigments, fillers, additives, and coatings in addition to the fiber particles [12]. Meanwhile, PTS contains high moisture (>98%) and fiber rejects (FR) contains very low moisture but also high ash content [10]. Regardless, all the PMS are wet, which prevent them from being applied directly for energy generation.

Hydrothermal carbonization (HTC) is an emerging technology for producing biofuels and upgrading solid fuels [15–18]. It conveniently uses residual moisture of the feedstocks as the reaction medium due to its solvent properties at high temperatures and pressures [19]. Therefore, wastes do not need to be dried prior to HTC, which is typically an energy intensive process. Subcritical water at around 200–260 °C has high ionic products and low dielectric constants, which allow water to be more reactive and cause it to behave similarly to non-polar solvents [20]. Therefore, HTC conditions allow for carbon based organic compounds (namely, hemicellulose and cellulose) to be hydrolyzed into monomers. These monomer fragments then undergo a series of reactions including dehydration, decarboxylation, condensation, and polymerization, which can result in products such as hydrochars and organic acids [15,16,21]. These reactions follow separate kinetics and can be catalyzed by acids, bases, and inorganics [22–24]. As a result of these complex reaction rates, a wide range of residence times ranging from 5 min to 6 h have been reported for HTC [18,25,26]. HTC process results in a solid hydrochar that is quite hydrophobic, friable, and energy dense [27–29]. Although temperature is considered as the most important processing parameter for an HTC process, the types of feedstock (e.g., herbaceous, woody, municipal sludge, food waste, sewage sludge, PMS, etc.) and their chemical compositions also determine the chemical characteristics of hydrochar [30–32]. As a result, different optimum HTC conditions are reported in the literature for different feedstocks [33–36]. Although large-scale implementation of HTC is yet to established, recent techno-economic analyses have shown that HTC of biomass can be economically viable and environmentally sustainable [37–39].

HTC of PMS has been extensively studied in the last few years. For instance, Areeprasert et al. performed HTC of PSS in a batch reactor at 180–240 °C for 30 min to determine optimal HTC conditions [40–42]. Afterwards, HTC was performed at the optimized condition (197 °C and 30 min) in a small pilot scale [43]. Their results indicate that HTC of PSS is energetically favorable in the context of Japan. Furthermore, the same group have determined combustion characteristics and combustion kinetics of PSS hydrochar and reported that the major decomposition was attributed for cellulose [44]. Meanwhile, the HTC process liquid resulting from PSS was analyzed and recycled in order to reduce the emission footprint of the paper mill [45]. In order to understand the HTC reaction parameters, Makela et al. performed HTC of PSS from 180–260 °C for 30 min–5 h, both with and without homogeneous catalysts [26,46]. Their results indicate that dehydration, depolymerization, and decarboxylation are more prominent than polymerization and aromatization. Similar to the other

biomass feedstocks, hydrochloric acids catalyzed HTC of PSS resulted in an energy yield increase of the hydrochar [46].

Literature has repeatedly used PSS or mixed sludge for HTC experiments, whereas the HTC of other PMS are rare and the differences in chemical compositions among the various PMS are likely to result in variations in hydrochars. Therefore, the goal of this study was to examine the fuel quality of solid hydrochars produced by various PMS at various HTC temperatures. The first objective of this study was to reveal whether the type of PMS feedstocks is more influential than the HTC temperature in terms of energy densification (ED). As the ultimate goal is to co-fire PMS hydrochar with coal in an existing coal-fired power plant, the second objective was to evaluate the combustion indices of the PMS hydrochars compared to the combustion indices of bituminous coal.

2. Materials and Methods

2.1. Materials

Six different PMS were obtained from an industrial partner's different pulp and paper mill plants found throughout the USA specifically for this study. Table 1 displays the samples names and how they are referenced throughout the manuscript. Samples PS, DPS, PSS_1, PSS_2, and PFR are all from different plants; PTS was obtained from the same plant as PFR samples. Meanwhile, Clarion #5a (bituminous coal) was used for co-combustion studies. All samples were dried in an oven at 105 °C for 24 h and sealed in Ziploc bags until further use. The nomenclature of the samples and their moisture contents are shown below in Table 1.

Table 1. Sample nomenclature used throughout manuscript and their respective moisture contents.

Sludge Sample	ID	MC (%)
Primary Sludge	PS	60.1 ± 1.5
De-inked Paper Sludge	DPS	63.5 ± 0.5
Primary and Secondary Sludge 1	PSS_1	64.1 ± 1.0
Primary and Secondary Sludge 2	PSS_2	76.5 ± 1.0
Primary Sludge and Fiber Rejects	PFR	57.1 ± 1.2
Pre-thickened Sludge	PTS	98.7 ± 0.1

2.2. Hydrothermal Carbonization (HTC)

All HTC experiments were performed in a 600 mL Parr 452HC3 Hastelloy reactor (Parr Instrument Company, Moline, IL, USA). Reactor temperature was controlled with a Parr 4843 proportional–integral–derivative controller (PID) controller using a J-type thermocouple with an accuracy of ± 3 °C. Reaction pressure was monitored as the reactor was a closed system, thus observed pressures were autogenous pressures in addition to the pressures exerted by produced gases. The reactor was loaded with a 1:9 dry sample to de-ionized (DI) water ratio. Once the reactor was sealed, the reactor stirrer was set to an RPM rate of 180 ± 2 rpm. The reactor mixtures were stirred from then until the end of the HTC process. The hydrochars were produced at reaction temperatures of 180 °C, 220 °C, and 260 °C. The reactor heating procedure was as follows: (1) the contents of the reactor were heated at approximately 8 °C min^{-1} until the set reaction temperature, (2) once at the target reaction temperature, the reactor temperature was held constant for a residence time of 30 min, (3) after the residence time, the reactor was submerged in an ice-water bath until it reached to 30 °C, which typically took around 10 min, and (4) reactor stirring was stopped once 30 °C was reached. Produced gases were vented in a fume hood and the process liquid was separated from the solid hydrochar via vacuum filtration and a Whatman 41 filter (20 μm). Hydrochar was washed with DI water until the pH of washed water reached the pH of DI water. The moist hydrochars were dried in an oven at 105 °C for 24 h, then stored in a Ziploc bag until further analysis.

2.3. Characterization of Hydrochars

Mass yields were calculated using Equations (1)–(3) and they show how much of the initial feedstock was converted into solid (hydrochar), liquid and gas.

$$\text{Solid Mass Yield (\%)} = \frac{\text{Mass of dry hydrochar}}{\text{Mass of untreated dry feedstock}} \times 100\% \tag{1}$$

$$\text{Liquid Mass Yield (\%)} = \frac{\text{Mass of liquid produced}}{\text{Mass of untreated dry feedstock}} \times 100\% \tag{2}$$

$$\text{Gas Mass Yield (\%)} = \frac{\text{Mass of gas produced}}{\text{Mass of untreated dry feedstock}} \times 100\% \tag{3}$$

Carbon, hydrogen, nitrogen, and sulfur content were determined using a Flash 2000 Organic Elemental Analyzer (Thermo Scientific, Grand Island, NY, USA). The oxygen content was calculated by subtracting carbon, hydrogen, nitrogen, sulfur, and ash percentages from 100%. Electrolytic copper and copper oxide were used for the analyzer's oxidation column and 2,5-Bis (5-tert-butyl-benzoxazol-2-yl) thiophene (BBOT) was used for calibration. Higher heating valued (HHV) were also determined for hydrochars using a Parr 6200 adiabatic oxygen-bomb calorimeter (Parr Instrument Company, Moline, IL, USA) calibrated with benzoic acid. Dry ash free HHV (HHV_{daf}) was calculated via Equation (4). Energy densification (ED) was calculated via Equation (5) to evaluate how HHV changes from the untreated feedstock to hydrochar.

$$HHV_{daf} = \frac{\text{HHV of the sample}}{1 - \text{Fraction of dry ash into the sample}} \tag{4}$$

$$ED = \frac{\text{HHV of dry hydrochar}}{\text{HHV of untreated dry feedstock}} \tag{5}$$

Lignin analysis was performed by the standard Technical Association of the Pulp and Paper Industry (TAPPI) method [47]. A modified method of Sequeira and Law [48] was used to quantify the sugar content. In this method, DI-water at 50 °C was used for making and blending a 5% solid slurry for one minute; three extractions were performed. Solid was filtered in a pressurized air filter (OFI Testing Equipment, model 140-31) by using Whatman no. 4 filter paper. The filtration process was operated just above atmospheric pressure to ensure liquor was extracted from the sludges or hydrochars. Final extraction was conducted in an autoclave (L30 cycle) to make sure no free sugar remained in the solid. HPLC (Agilent 1200 series) was used to analyze the sugar and sugar alcohols. HPLC was equipped with a binary pump, an HPX-87P (Bio-Rad) column, and a refractive index (RI) detector. Water was used as a mobile phase with a flowrate of 0.5 mL min^{-1}. The column was heated to 85 °C to enhance the separation and the RI detector was used at 55 °C. An external calibration was used to quantify the contents (lactose, glucose, xylose, galactose, arabinose, mannose, and fructose).

Volatile matter, fixed carbon, and ash content of samples were determined by thermogravimetric analyses (TGA) using a TGA Q500 (TA instruments, New Castle, DE, USA). Sample heat rate was set at 20 °C min^{-1} and all gas flowrates were set at 50 mL min^{-1}. A nitrogen atmosphere was used for proximate analysis. Samples were heated from 25 °C to 105 °C and held at 105 °C for 5 min, the temperature was then increased to 900 °C and then held for 5 min. Air was then introduced for 10 min to combust the remaining sample left at 900 °C. The mass loss under the nitrogen atmosphere at 105 °C was considered moisture. Mass loss between 105 °C and 900 °C were considered volatile matters. Mass remaining at the end of the combustion process was considered ash. Fixed carbon was determined by subtracting moisture, volatile and ash percentages from 100%.

Oxidative reactivity was performed to determine fuel properties and was performed similarly to the proximate analysis method described earlier using the same equipment. Similar heating rates, gas flows, and temperature increments were used, but air was the only gas used during the entire

run. Combustion thermograms and derivative of the mass relative to temperature (DTG) curves were plotted as shown in the literature [49]; calculation of ignition (Equation (6)) and burnout (Equation (7)) indices are presented below [50]:

$$D_i = \frac{|DTG_{max}|}{t_p t_i} \tag{6}$$

$$D_B = \frac{|DTG_{max}|}{\Delta t_{1/2} t_p t_B} \tag{7}$$

where, DTG_{max} is the maximum rate of combustion, in magnitude, found in the combustion DTG curves; t_p is the time where DTG_{max} occurs; t_i and t_B are the time at which the ignition temperatures and burnout temperatures are obtained, respectively; and $\Delta t_{1/2}$ is the time when the combustion DTG value is one-half of the DTG_{max}. Lower values of D_i and D_B indicate an ideal ignition and burnout (i.e. overall combustion) behavior.

3. Results and Discussion

3.1. Product Distribution and Energy Densification

Table 2 shows the solid, liquid, and gas mass yields of with respect to different HTC temperatures. The initial solid to liquid ratio for each experiment was maintained at 1:9. With the increase of HTC temperature, liquid percentage increases and at the same time solid percentage decreases in the output. The increase of liquids resulted from the decomposition reactions that occur during HTC; mainly in the form of dehydration, polymerization, and aromatization reactions [21,51]. Although there was no gas added initially in the reactor, a small amount of gas (less than 1 g total) had been generated during HTC, especially at higher HTC temperatures. Decarboxylation of PMS polymers may resulted in the gaseous product [21,52]. Since the reactivity of biomass increases with the HTC temperature, lower solid mass yields were expected with the increase of HTC temperatures.

Table 2. Mass yields and energy densification of paper mill sludges (PMS) and their hydrochars ([a] Not applicable).

Sample	HTC Temperature (°C)	Solid Mass Yield (%)	Liquid Mass Yield (%)	Gas Mass Yield (%)	HHV$_{daf}$ (MJ kg^{-1})	ED
PS	Raw	NA [a]	NA [a]	NA [a]	15.5 ± 0.0	NA [a]
	180	96.2 ± 2.0	3.8 ± 2.0	0.0 ± 0.0	15.1 ± 0.4	1.0 ± 0.0
	220	85.4 ± 2.0	11.8 ± 2.2	2.8 ± 0.2	15.3 ± 0.4	1.0 ± 0.0
	260	30.3 ± 1.1	58.1 ± 2.4	11.6 ± 1.4	22.8 ± 0.1	1.5 ± 0.0
DPS	Raw	NA [a]	NA [a]	NA [a]	13.0 ± 0.0	NA [a]
	180	91.7 ± 0.9	8.3 ± 0.9	0.0 ± 0.0	13.0 ± 0.2	1.0 ± 0.0
	220	84.4 ± 0.9	13.3 ± 1.4	2.3 ± 0.5	12.9 ± 0.1	1.0 ± 0.0
	260	58.4 ± 2.0	33.9 ± 1.3	7.2 ± 1.3	11.4 ± 0.7	0.9 ± 0.1
PSS$_1$	Raw	NA [a]	NA [a]	NA [a]	21.4 ± 0.1	NA [a]
	180	81.2 ± 0.3	18.3 ± 1.0	0.0 ± 0.0	21.7 ± 0.1	1.0 ± 0.0
	220	74.1 ± 0.0	22.2 ± 0.4	3.6 ± 0.5	21.7 ± 0.1	1.0 ± 0.0
	260	54.1 ± 2.0	38.8 ± 3.6	7.1 ± 1.6	27.4 ± 0.1	1.3 ± 0.0
PSS$_2$	Raw	NA [a]	NA [a]	NA [a]	19.6 ± 0.2	NA [a]
	180	90.9 ± 0.5	9.1 ± 0.5	0.0 ± 0.0	19.6 ± 0.1	1.0 ± 0.0
	220	78.9 ± 1.2	18.4 ± 1.2	2.7 ± 0.0	20.2 ± 0.1	1.0 ± 0.0
	260	41.1 ± 1.7	49.9 ± 2.1	9.0 ± 0.4	28.9 ± 0.1	1.5 ± 0.0
PFR	Raw	NA [a]	NA [a]	NA [a]	19.7 ± 0.2	NA [a]
	180	93.2 ± 2.1	6.8 ± 2.1	0.0 ± 0.0	18.5 ± 0.0	0.9 ± 0.0
	220	81.9 ± 1.2	15.6 ± 0.5	2.5 ± 0.7	19.3 ± 0.2	1.0 ± 0.0
	260	45.4 ± 1.2	42.9 ± 0.8	10.7 ± 0.4	25.2 ± 0.3	1.3 ± 0.0
PTS	Raw	NA [a]	NA [a]	NA [a]	17.1 ± 0.7	NA [a]
	180	87.5 ± 2.9	8.0 ± 0.8	0.0 ± 0.0	18.6 ± 0.5	1.1 ± 0.0
	220	69.8 ± 2.8	25.2 ± 1.4	5.0 ± 1.4	21.6 ± 0.1	1.3 ± 0.0
	260	43.8 ± 1.1	52.0 ± 4.6	4.1 ± 3.5	31.5 ± 3.7	1.8 ± 0.3
Clarion # 5a coal	Raw	NA [a]	NA [a]	NA [a]	30.5 ± 0.3	NA [a]

The variation of HTC product distribution resulting from different PMS feedstocks can be found in Table 2. Solid mass yields of HTC treated PSS_1 and PSS_2 considerably decreased as reaction temperature increased, reaching yields as low as 54.1% and 41.1%, respectively at 260 °C. Even though both are mixtures of primary and secondary sludges, their solid mass yields were significantly different. The reason could simply be the variation of ratios of primary to secondary sludges in the samples. This result shows that sludge feedstocks can vary in a manner that impacts HTC performance, even amongst the same category of sludges. The yields at 180 °C and 220 °C were quite high for both feedstocks, which may indicate that both sludges were rich in cellulose and lignin. As the cellulose and lignin react with water during HTC at approximately 220–230 °C and 255–265 °C, respectively, PMS remain mostly unreacted at 180 °C and 220 °C [52–55]. So far, researchers have mainly conducted their research on the mixed (primary and secondary) PMS and have found the solid mass yield in a range between 29 to 65% depending on the mixing ratio of primary to secondary sludges when the HTC was conducted at 260 °C [26,56].

Solid mass yield of HTC treated PS significantly decrease at the high reaction temperature, reaching a yield as low as 30.3% at 260 °C. However, minimal changes were observed at 180 and 220 °C, which indicate that the PS is rich in cellulosic material that did not completely react until 260 °C. Kim et al. found that the PS contains 58% cellulose [57]. The solid mass yield of PFR was similar to PS at low temperatures (180 and 220 °C), while solid mass yield of PFR was higher than the solid mass yield of PS at 260 °C. The reason for this higher solid mass yield for PFR could be the presence of higher lignocellulosic material in PFR compared to PS, as PFR contains tree branches and barks. These lignin-rich compounds breakdown slowly, and likely remain unreacted at these treatment conditions.

Since PTS is basically the PS prior to the dewatering step [14], the solid mass yield for PTS are expected to be similar to PS. However, a significant difference was observed between their solid mass yields, especially at 260 °C. The solid mass yield was 43.8% for PTS while it was 30.3% for PS. Although the yields were different, they fall within the literature values of PS (29 to 65%). This difference indicates that the PTS might have an even distribution of lignin and cellulosic compounds, as it seems similar to degradation from 180 °C to 220 °C to 260 °C. With PS, more significant difference occurs between 220 °C and 260 °C than between 180 °C and 220 °C. This indicates that the PS is composed of more hardy lignin compounds that break down at higher temperatures. These differences in solid mass yield with respect to temperature are consistent with previous literature, which has traditionally explained this observation as being the result of difference in feedstocks. A mild change in solid mass yield at 260 °C was observed for DPS, which was 58.4%. This higher solid mass yield, compared to the other sludges, may be due to either the sludge containing more inorganic components which remain unreacted during HTC, or the sludge containing more lignocellulosic fiber wastes which do not degrade as readily under these conditions.

It was observed from the mass yields that minimal carbonization happened to the PMS at 180 °C and 220 °C, even though cellulose degradation is expected to occur at 220 °C. Meanwhile, significant changes only happened to all PMS at 260 °C. This indicates that the cellulosic mass may be stabilized by the other lignin components in the PMS, requiring a higher temperature to initiate the HTC process. Mass yields alone, however, do not give a full account of the benefits of the HTC process. As the main focus of this study is the fuel properties of solid hydrochars, it is necessary to check additional fuel characteristics (i.e., HHV or ED) of all hydrochars to evaluate the more impactful hydrochars for further analysis.

How the energy is concentrated into the hydrochar with respect to its raw sample is known as energy density (ED). The dry ash-free HHV (HHV_{daf}) and ED, relative to the raw samples, are shown in Table 2. The HHV_{daf} of raw sludges varies from 13.0 to 21.4 MJ kg^{-1}, where DPS has the minimum, PSS_1 has the maximum, and the others fall in between. The HHV_{daf} of all sludges are lower than the HHV of bituminous coal (25.4–27.4 MJ kg^{-1}) [58,59]. The HHV_{daf} of hydrochars produced at 180 and 220 °C were similar to their individual raw samples. However, the HHV_{daf} of hydrochars produced at 260 °C were significantly higher than the corresponding raw samples, with the exception of DPS. Some

of them are even higher than the HHV_{daf} of coal (e.g., hydrochar of PSS_1, PSS_2, and PTS produced at 260 °C). The HHVs of hemicellulose and cellulose have a range between 16.8–18.6 MJ kg^{-1} and break down around 180 °C and 220–230 °C [53,54,60]. On the other hand, lignin not only has a higher HHV (23.3–25.6 MJ/kg) but also has HTC initiation around 255–265 °C [52,55]. As a result, the component that has higher HHV stays in the hydrochar product at a higher HTC temperature. The only exception was observed in DPS, where the HHV decreases with the increase of HTC temperature. This decrease in HHV, which is unique to the DPS char, is due to the loss of carbon and relative increase in oxygen (both must be compared to the total mass loss of the sludge). The lack of carbonization could be due to the higher amount of inorganics present in the DPS, which is shown in its high ash content.

Table 2 shows that ED remains 1.0 for all hydrochars produced at 180 and 220 °C, which indicates that almost nothing favorable happened for PMS in terms of energy content at those HTC conditions. However, the energy contents by the hydrochars produced at 260 °C were 1.3 to 1.8 times higher than their raw samples except for DPS, which had ED lower than 1.0 at 260 °C. As such, the types of feedstocks are more significant than HTC reaction temperature for densifying the energy in PMS. As solid fuel properties of PMS are the main focus of this study and significant changes of ED happened only at HTC 260 °C, from now on, the characteristics of hydrochars produced at 260 °C will be discussed in the following sections.

3.2. Chemical Characteristics of PMS Hydrochars Produced at 260 °C

From the previous sections, it was observed that the solid mass yield decreases and ED generally increases with the HTC temperature. Therefore, it is important to evaluate how the organics and lignin in the hydrochars produced at 260 °C vary from their raw sludges, including their significant impact on ED. Table 3 presents the ultimate analysis including ash, lignin, and sugar (C_5 and C_6) content of all PMS and their corresponding hydrochars produced at 260 °C. Hydrochar of each sample has higher carbon content compared to its raw sample, except DPS. The carbon content increases from 34.6% to 44.3%, 38.4% to 40.5%, 42.8% to 62.2%, 39.8% to 57.6%, and 23.9% to 40.2% for PS, PSS_1, PSS_2, PFR, and PTS, respectively. However, this content decreases for DPS from 27.1% to 22.2%. The oxygen content, on the other hand, has a decreasing trend for all sludges from raw to its hydrochar. The oxygen content decreases from 44.4% to 18.5%, 37.0% to 29.6%, 30.3% to 16.0%, 45.8% to 25.0%, 34.6% to 9.2%, and 48.4% to 3.3% for PS, DPS, PSS_1, PSS_2, PFR, and PTS, respectively. The loss of hydroxyl groups due to the dehydration reaction during HTC results in lower the oxygen content [58]. The increase in carbon and a decrease in oxygen content complement the HHV increases after HTC treatment. Although the oxygen content decreases for DPS, the carbon content also decreases with HTC, resulting in the decrease of HHV. Hydrogen and nitrogen content change minimally and remain approximately the same. Fuel qualities of the PMS hydrochars were further analyzed with van-Krevelen diagram (Figure 1). In the van-Krevelen diagram, a sample closer to the origin indicates a higher quality fuel (i.e., anthracite) and a sample far from the origin specifies a poor-quality fuel (i.e., lignite or biomass). Fuel quality of all PMS except DPS being vastly upgraded with HTC at 260 °C and falls between bituminous and sub-bituminous region shown in Figure 1.

Ash content in each hydrochar was higher from its raw sample shown in Table 3. Ash is predominantly inert in the HTC process, so it is expected to become concentrated as the HTC process progresses. Higher ash content in treated samples is a result of HTC breaking down organic biomass constituents (release into liquid phase) and keep concentrating the inorganic content in the solid phase [25,61]. Similar to the ash content, lignin content was also higher in hydrochar compared to its raw sludge. This number increases from 5.2% to 36.9%, 10.0% to 19.7%, 20.2% to 46.8%, 17.6% to 87.8%, 22.6% to 57.9%, and 20.4% to 44.2% for PS, DPS, PSS_1, PSS_2, PFR, and PTS, respectively. As lignin breaks down between 255–265 °C [52,55], unreacted lignin is concentrated in the solid phase. Higher lignin content in hydrochar can be supported by the increase in HHV for most sludges following treatment as a result of reactive, less energy dense cellulose being removed from the char more at higher temperatures.

Total sugar content in raw samples and their hydrochar was almost the same, shown in Table 3. The short-chain sugar molecules (C_5 and C_6) are likely the product of hydrolyzed cellulose and hemicellulose [62]. However, these sugar molecules are highly reactive at HTC conditions and they tend to dehydrate into furan derivatives (e.g., furfural, hydroxymethyl furfural etc) or decarboxylated to short-chain acids, CO_2 and water [62]. However, in PMS, the number did not increase, which could indicate that dehydration and decarboxylation of sugars are more dominant than hydrolysis of PMS.
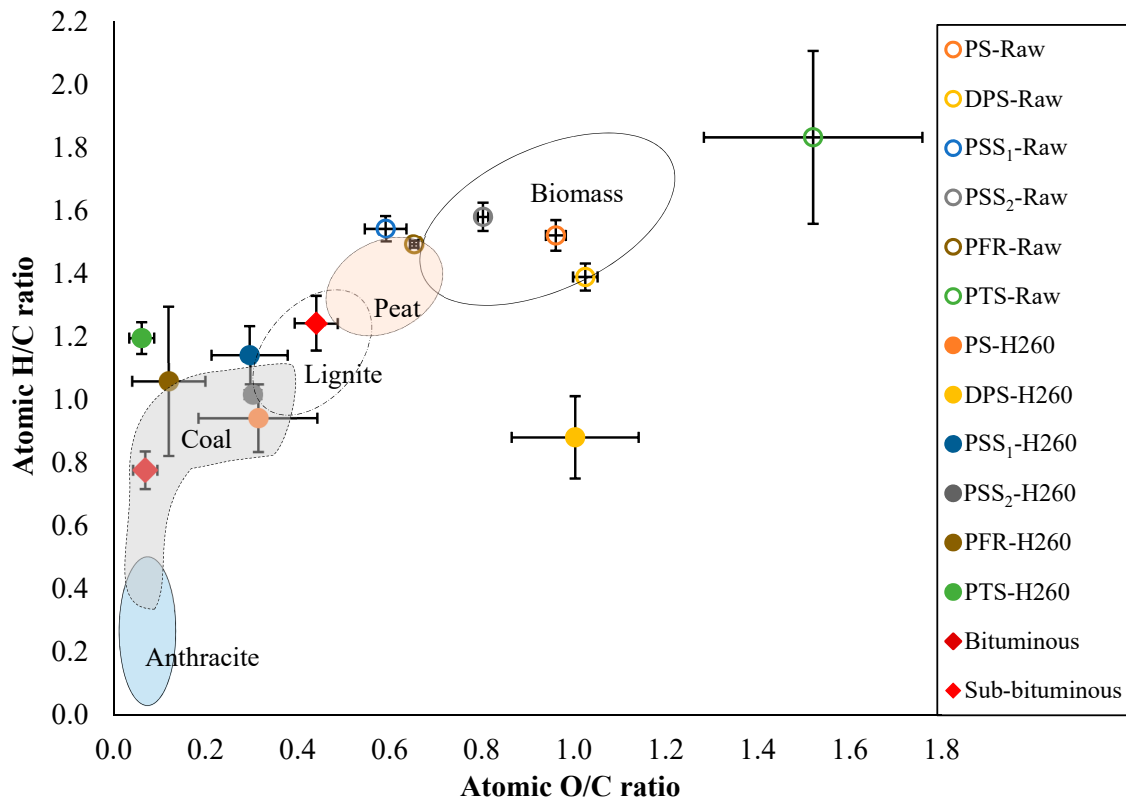
Figure 1. van-Krevelen diagram for all raw and hydrochar samples including bituminous and sub-bituminous coal.

Table 3. Ultimate analysis, ash and lignin number for all raw and hydrochar samples ([a] indicates that it was calculated by difference; [b] Below detection limit; and [c] Not applicable).

Sample	HTC Temperature (°C)	Carbon (%)	Hydrogen (%)	Nitrogen (%)	Sulfur (%)	Oxygen [a] (%)	Ash (%)	Lignin (%)	C_5 and C_6 Sugar (mg/g)
PS	Raw	34.6 ± 0.4	4.7 ± 0.1	0.3 ± 0.0	BD [b]	44.4 ± 0.8	16.0 ± 0.0	5.2 ± 0.4	2.7 ± 0.3
	260	44.3 ± 3.3	3.8 ± 0.3	0.2 ± 0.0	2.0 ± 0.0	18.5 ± 7.5	33.1 ± 1.7	36.9 ± 1.3	3.0 ± 0.3
DPS	Raw	27.1 ± 0.2	3.4 ± 0.1	0.7 ± 0.0	BD [b]	37.0 ± 0.9	31.9 ± 0.4	10.0 ± 1.2	2.0 ± 0.2
	260	22.2 ± 1.7	1.8 ± 0.2	0.4 ± 0.1	0.1 ± 0.0	29.6 ± 3.4	46.0 ± 0.3	19.7 ± 0.8	1.9 ± 0.3
PSS_1	Raw	38.4 ± 0.8	5.3 ± 0.1	2.3 ± 0.2	0.9 ± 0.1	30.3 ± 2.2	22.8 ± 0.4	20.2 ± 0.1	4.0 ± 1.1
	260	40.5 ± 1.5	4.2 ± 0.3	2.1 ± 0.0	1.3 ± 0.0	16.0 ± 4.4	36.0 ± 1.3	46.8 ± 0.8	1.4 ± 0.0
PSS_2	Raw	42.8 ± 0.0	6.1 ± 0.2	0.7 ± 0.1	0.2 ± 0.0	45.8 ± 0.7	4.5 ± 0.1	17.6 ± 0.5	3.5 ± 1.2
	260	62.2 ± 0.7	5.7 ± 0.1	1.6 ± 0.1	0.3 ± 0.0	25.0 ± 1.5	5.2 ± 0.1	87.8 ± 5.9	3.5 ± 2.5
PFR	Raw	39.8 ± 0.1	5.3 ± 0.0	0.6 ± 0.1	0.3 ± 0.0	34.6 ± 0.5	19.5 ± 0.1	22.6 ± 0.3	3.8 ± 2.2
	260	57.6 ± 2.6	5.5 ± 1.2	0.6 ± 0.1	0.4 ± 0.1	9.2 ± 6.1	26.8 ± 0.3	57.9 ± 1.2	2.8 ± 0.3
PTS	Raw	23.9 ± 2.7	3.9 ± 0.4	0.6 ± 0.0	6.2 ± 0.6	48.4 ± 5.2	17.1 ± 0.1	20.4 ± 0.5	3.2 ± 2.2
	260	40.2 ± 1.4	4.3 ± 0.1	0.4 ± 0.1	1.3 ± 0.2	3.3 ± 1.5	50.5 ± 1.5	44.2 ± 0.6	2.4 ± 1.2
Clarion # 5a coal	Raw	63.8 ± 1.2	4.1 ± 0.1	1.5 ± 0.0	4.6 ± 0.8	14.9 ±	11.1 ± 0.6	NA [c]	NA [c]
Bituminous coal [63]	Raw	75.1 ± 2.8	5.3 ± 0.4	1.5 ± 0.1	1.1 ± 0.8	6.9 ± 2.6	10.0 ± 1.4	NA [c]	NA [c]
Sub-bituminous coal [64]	Raw	55.8 ± 3.5	6.2 ± 0.2	0.7 ± 0.1	0.3 ± 0.1	32.7 ± 2.8	4.3 ± 0.9	NA [c]	NA [c]

3.3. Fuel Characteristics of Hydrochars

Carbon contents in the PMS hydrochars were increased with HTC, while oxygen contents were decreased, resulting in increases of HHV_{daf}. While this increase makes the hydrochars more similar to bituminous coal, another factor to consider is that there is clearly a wide range of ash contents observed in PMS samples, which will impact fuel quality. Additionally, combustion properties of those hydrochars are required to further evaluate the fuel characteristics in order to determine the feasibility of co-combustion with coal. Pyrolysis thermograms of various hydrochars, shown in Figure 2, illustrates the thermal gravimetric (TG) curves and derivative thermal gravimetric (DTG) curves for hydrochars produced at 260 °C from PS, DPS, PSS_1, PSS_2, PFR, and PTS with respect to TG pyrolysis temperatures. The TG curves for PS-H260, PSS_2-H260, PFR-H260, and PTS-H260 showed a rapid mass loss between 190 to 550 °C with a maximum mass loss rate of -4.14, -7.86, 6.05, and -6.48% min^{-1}, respectively. This rapid mass loss could be attributed to the high volatile materials present in these hydrochars [65]. The PSS_2-H260 lost 61% of its initial mass during the complete pyrolysis stage which was the maximum among others while the PS-H260, PFR-H260 and PTS-H260 have lost 51%, 55%, and 43%, respectively. Although PSS_1 and PSS_2 both are mixtures of primary and secondary sludges, the TG curve of PSS_1-H260 exhibited a slow mass loss for the same temperature range with a maximum mass loss rate of -3.21% min^{-1} compared to PSS_2-H260 and lost 46% of its initial mass. This is another confirmation that the sources of these samples were different and/or the ratios of primary to secondary sludges are not the same. The TG curve of DPS-H260 displayed a maximum mass loss rate of -7.13% min^{-1} at a much higher temperature range of 640–780 °C. The presence of higher inorganic compounds or lignin could be the possible reason for this shift towards higher temperature compared to other sludges [66]. The TG curve for PS, which is dewatered PTS [14], also illustrated its maximum mass loss rate in this temperature range.
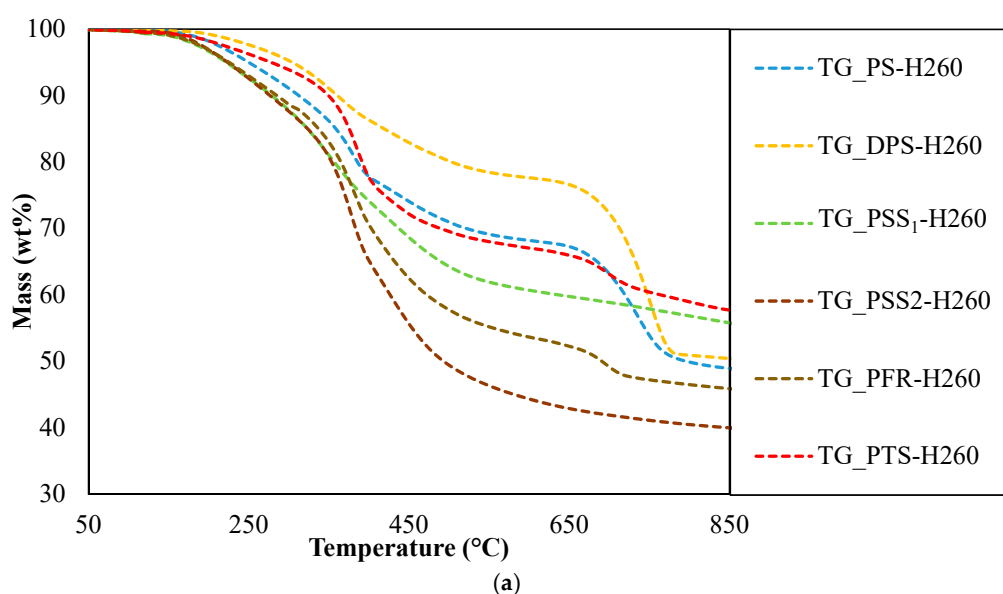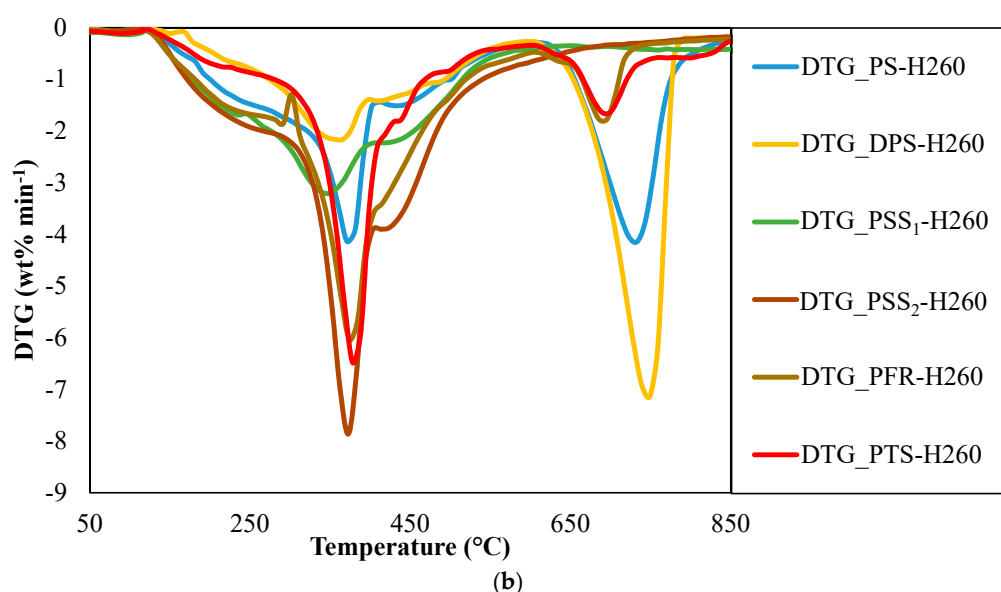

(**a**)

Figure 2. *Cont.*

(**b**)

Figure 2. Pyrolysis thermograph plotted versus temperature (**a**) and derivative thermal gravimetric (DTG) curves plotted versus temperature (**b**) for all 260 °C hydrothermal carbonization (HTC) treated paper mill sludges (PMS).

The DTG curves for all the hydrochars, except for PSS$_1$-H260 and PSS$_2$-H260, showed two distinct peaks at two different temperature ranges of 310–400°C and 640–780°C, respectively. The DTG curves of PSS$_1$-H260 and PSS$_2$-H260 displayed only one major peak in between 310–400 °C. All DTG curves have minor peaks after the major peak in the temperature range of 310–400°C. The origin of these peaks can be explained from the constituents of PMS. Yanfen et al. [66] stated that paper pulp and fiber are the main organic elements of PMS and because of the degradation of hemicellulose, cellulose, and lignin present in the sludges are primarily responsible for these peaks. Previous studies have also found that hemicellulose decomposes between 200–300 °C during pyrolysis, while cellulose decomposes between 300–400 °C. The pyrolysis of lignin starts above 300 °C and continues for a wide temperature range [58]. All the peaks illustrated in DTG curve of Figure 2b agree with these findings. The peaks before 400 °C attributed to the complete decomposition of hemicellulose and cellulose and partial decomposition of lignin as it degrades over a wide range of pyrolysis temperature. The peaks after 400 °C correspond to the complete breaking of lignin [50]. However, the second peak for PS and DPS emerged at 750 °C. The pyrolysis of chemicals (i.e., additives, coagulants, flocculants, CaCO$_3$, and other minerals) present in the PS and DPS could be the possible reason for the emergence of the second peak at a higher temperature compared to other sludges [66,67].

The proximate analysis of various raw and PMS hydrochars at 180, 220, and 260 °C are presented in Figure 3. The figure indicates that the raw PMS samples were high in volatile matters and low in fixed carbon. Among the raw PMS samples, PSS$_2$ contained the highest volatile matters and the lowest ash while PSS$_1$ had the highest fixed carbon. Figure 3 also shows the change of ash, fixed carbon, and volatile matters present in various sludges with respect to HTC temperatures compared to raw samples. The figure also illustrates that HTC of PMS at 180 and 220 °C did not significantly affect the volatile materials, fixed carbon, and ash content compared to raw PMS samples, which have already been discussed in Section 3.1. However, the ash and fixed carbon were increased and volatile matters of PMS decreased remarkably when HTC temperature increased from 220 °C to 260 °C. The presence of high inorganic materials, which were trapped in the solid phase of the product instead of being leached in to the liquid phase, could be a possible reason for the increase in ash. The decrease in volatile materials could be attributed to the decomposition of cellulose and hemicellulose producing gaseous species like CO, CO$_2$, and short-chained hydrocarbons [66,68]. The decomposition of volatile

materials also increased the fixed carbon in 260 °C hydrochars [69]. Among the PMS hydrochars, PSS$_2$ contained the maximum volatile materials and fixed carbon as well as the lowest ash percentage.
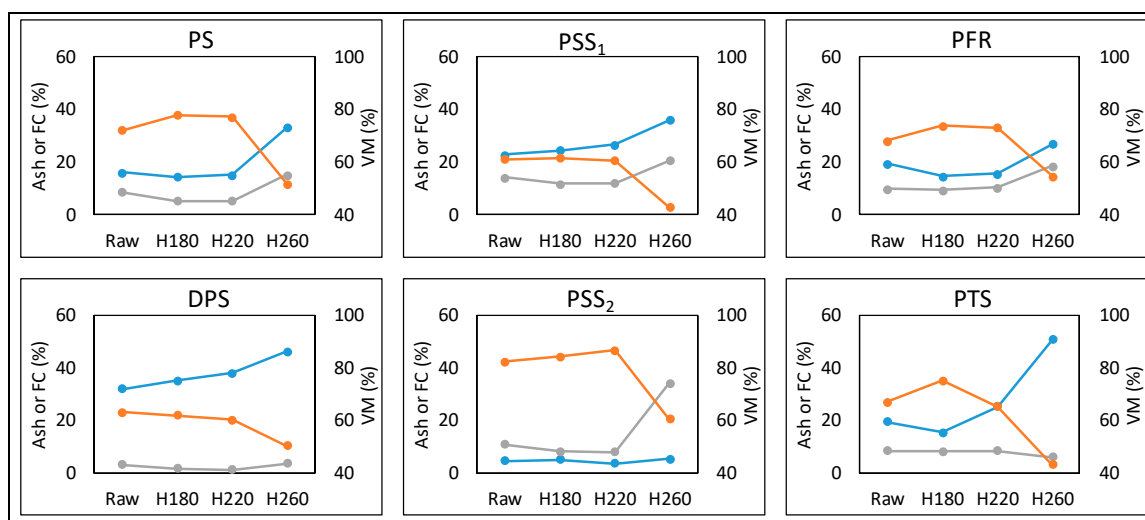

Figure 3. Proximate analysis of various paper mill sludges hydrothermally carbonized at 180–260 °C. The orange, gray, and blue lines represent volatile matter (VM), fixed carbon (FC) and ash content, respectively.

Figure 4 shows the co-combustion thermograph of coal, hydrochar of one paper mill sludge PTS, at 260 °C and their 50-50 mix. These parameters were selected because the PTS hydrochar saw the greatest energy densification at 260°C. Additionally, 50% mass should allow for both components to show combustion characteristics to determine if any positive or negative synergistic effects exist during co-firing. The PTS hydrothermally treated at 260 °C was co-combusted with coal to examine the combustion characteristics through TG curve and first negative derivative of DTG curve. The TG curve of this PTS hydrochar showed a rapid mass loss of approximately 60% from 170–350 °C. This rapid mass loss occurred due to the presence of high volatile materials (~45%) in PTS hydrochar [59]. However, the TG curve for coal displayed a comparatively slow mass loss from 170–608°C as it contained lower volatile materials than PTS hydrochar treated at 260 °C. The combustion TG curve for the mix followed a trend similar to the coal TG curve as it showed a slow mass loss in the same temperature range as coal. The DTG curve for PTS hydrochar indicated a maximum mass loss rate of -35.71% min^{-1} at 317 °C whereas coal DTG curve showed the maximum mass loss rate at a higher temperature of 537 °C. The mix DTG showed a combustion characteristic more like the coal where the maximum mass loss occurred at 541 °C. It is observed from Figure 4 that the combustion of 50-50 mix of PTS hydrochar and coal was more similar to the coal combustion than to PTS combustion.
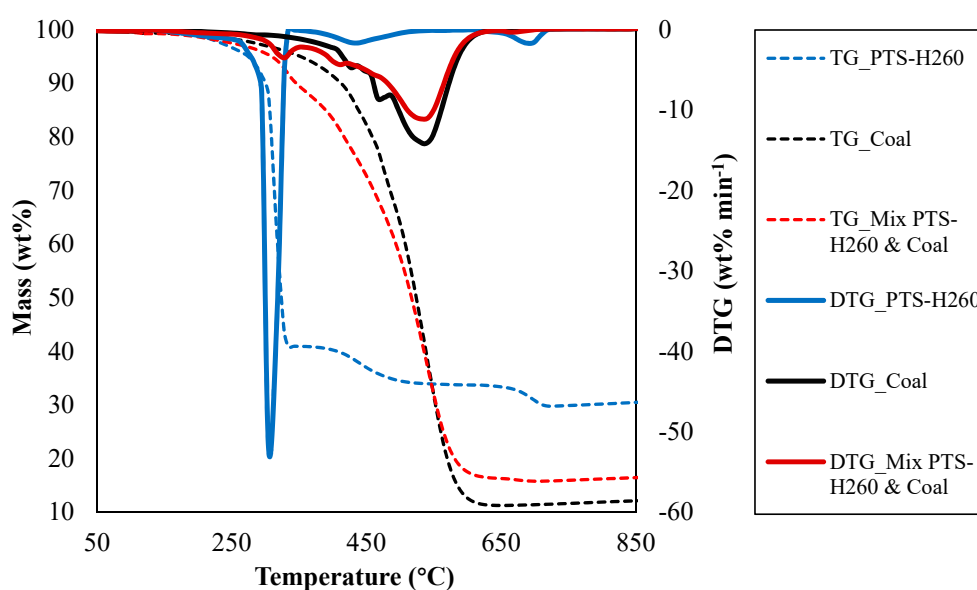
Figure 4. Combustion thermograph and DTG curves plotted versus temperature for 260 °C HTC treated paper mill sludges, coal and 50% mixtures of coal and hydrochar (TG nomenclature refers to mass loss on the left axis and DTG can be found on the right axis).

Additional efforts were made to analyze the combustion characteristics of Clarion # 5a coal (volatile matter (VM) and fixed carbon (FC) are 34.3 ± 0.0 and 54.0 ± 0.5, respectively), all the HTC-260 hydrochars and their 50-50 (wt% dry basis) mix with coal. During co-combustion, DPS-H260 was not considered as it has low ED compared to other PMS as discussed in earlier sections. All the parameters of combustion characteristics are presented in Table 4. Ignition and burnout indices were calculated using Equations (6) and (7). The ignition temperatures for all the hydrochars produced at 260 °C, except for DPS-H260, were low compared to coal as they contain high volatile material than coal [70]. The presence of high inorganics in DPS could be a reason for high ignition temperature. The other combustion parameters of the same hydrochar also deviated a lot compared to coal. However, when other 260's hydrochars were mixed with coal, these deviations became small. For example, before mixing, the values of ignition temperature, ignition time, burnout temperature, burnout time, DTG_{max}, DTG_{max} time, ignition and burnout indices for PTS-H260 were 294.2 °C, 20.3 min, 342.8 °C, 22.8 min, -52.1% min^{-1}, 20.8 min, 1.24×10^{-1}, and 5.40×10^{-3}, respectively. When mixed with coal, these values became 430.5 °C, 26.8 min, 692.0°C, 39.8 min, -11.1% min^{-1}, 31.8 min, 1.31×10^{-2}, and 3.12×10^{-4}, respectively, which were close to the values for coal. However, in the case of PS-H260, the deviations were still large even though the DTG_{max} value became closer than all the other hydrochars. As such, it is evident from Table 4 that combusting hydrochar produced from PMS at 260 °C (except PS) with coal made had a co-combusting characteristic that is similar to coal.

Table 4. Combustion Characteristics of determined from Combustion TGA data. (Clarion #5a coal (bituminous) was used for co-combustion [59]).

Sample	Ignition Temperature (°C)	Ignition Time (min)	DTG_{max} (% min^{-1})	Burnout Temperature (°C)	Burnout Time (min)	DTG_{max} Time (min)	Ignition Index, D_i	Burnout Index, D_B
PS-H260	380.4	23.8	−19.4	752.5	42.3	25.8	3.17×10^{-2}	7.19×10^{-4}
DPS-H260	628.1	36.3	−6.6	788.7	44.3	41.8	4.39×10^{-3}	9.10×10^{-5}
PSS$_1$-H260	262.0	18.8	−8.6	606.4	35.8	20.8	2.21×10^{-2}	5.88×10^{-4}
PSS$_2$-H260	273.0	19.3	−41.7	557.1	33.3	19.8	1.10×10^{-1}	3.26×10^{-3}
PFR-H260	294.1	20.3	−38.0	708.4	40.8	21.3	8.82×10^{-2}	2.10×10^{-3}
PTS-H260	294.2	20.3	−52.1	718.5	41.3	20.8	1.24×10^{-1}	2.98×10^{-3}
Coal	466.7	28.8	−14.2	627.8	36.8	32.3	1.53×10^{-2}	4.19×10^{-4}
50% Coal + 50% PS-H260	305.3	20.8	−14.5	739.4	42.3	21.8	3.22×10^{-2}	7.49×10^{-4}
50% Coal + 50% PSS$_1$-H260	386.3	24.8	−7.0	648.0	37.8	31.8	8.97×10^{-3}	2.10×10^{-4}
50% Coal + 50% PSS$_2$-H260	398.7	24.8	−9.9	660.3	37.8	31.3	1.28×10^{-2}	3.16×10^{-4}
50% Coal + 50% PFR-H260	410.3	25.3	−7.5	701.8	39.8	31.8	9.38×10^{-3}	2.46×10^{-4}
50% Coal + 50% PTS-H260	430.5	26.8	−11.1	692.0	39.8	31.8	1.31×10^{-2}	3.12×10^{-4}

4. Conclusions

Six different paper mill sludges have been hydrothermally carbonized at 180 °C, 220 °C, and 260 °C. With the exception of DPS; HHV_{daf} and ED ratio were maximized at HTC temperature of 260 °C for all the PMS. Although PMS sludges showed two-staged thermal degradation during pyrolysis, the thermograms revealed that hydrochars produced from different PMS possess different degradation severity. While, primary and secondary mix sludges show lower solid mass yields at lower HTC temperatures, the deinked primary sludge shows a higher solid mass yield at similar HTC conditions. Moreover, primary and secondary sludge samples showed anomalies in thermograms between themselves. The combustion indices indicate that hydrochar produced from paper mill sludges have lower ignition temperatures and higher burnout temperatures than raw bituminous coal. However, co-firing with coal and hydrochar showed higher ignition temperatures and lower burnout temperatures. Moreover, most of the hydrochars, specifically hydrochars from primary and secondary sludge, have shown very similar combustion thermograms to coal. In addition, by considering the ash content in the feedstocks and their hydrochars, PSS_2 could be a suitable co-fired option in existing coal-fired power plants.

References

1. Shaykheeva, D.; Panasyuk, M.; Malganova, I.; Khairullin, I. World Population Estimates and Projections: Data and Methods. *J. Econ. Econ. Educ. Res.* **2016**, *17*, 237–247.
2. Annual Energy Outlook 2016. Available online: http://large.stanford.edu/courses/2016/ph240/martelaro1/docs/0383-2016.pdf (accessed on 5 March 2019).
3. United States Department of Energy. *Billion Ton Update: Biomass Supply for a Bioenergy and Bioproducts Industry*; Oak Ridge National Laboratory: Oak Ridge, TN, USA, 2016.
4. Bird, M.; Talberth, J. *Waste Stream Reduction and Re-Use in the Pulp and Paper Sector*; Washington State Department of Ecology: Santa Fe, NM, USA, 2008.
5. Aspitarte, T.R.; Rosenfield, A.S.; Smale, B.C.; Amberg, H.R. *Methods for Pulp and Paper Mill Sludge Utilization and Disposal*; USEPA: Washington, DC, USA, 1973.
6. Mun, T.Y.; Tumsa, T.Z.; Lee, U.; Yang, W. Performance evaluation of co-firing various kinds of biomass with low rank coals in a 500 MWe coal-fired power plant. *Energy* **2016**, *115*, 954–962. [CrossRef]
7. Tsai, M.-Y.; Wu, K.-T.; Huang, C.-C.; Lee, H.-T. Co-firing of paper mill sludge and coal in an industrial circulating fluidized bed boiler. *Waste Manag.* **2002**, *22*, 439–442. [CrossRef]
8. Bajpai, P. Generation of Waste in Pulp and Paper Mills. In *Management of Pulp and Paper Mill Waste*; Springer International Publishing: Basel, Switzerland, 2015.
9. Monte, M.C.; Fuente, E.; Blanco, A.; Negro, C. Waste management from pulp and paper production in the European Union. *Waste Manag.* **2009**, *29*, 293–308. [CrossRef] [PubMed]
10. IPPC. *Reference Document on Best Available Techniques in the Pulp and Paper Industry*; European IPPC Bureau: Seville, Spain, 2001.
11. Soucy, J.; Koubaa, A.; Migneault, S.; Riedl, B. Chemical Composition and Surface Properties of Paper Mill Sludge and their Impact on High Density Polyethylene (HDPE) Composites. *J. Wood Chem. Technol.* **2016**, *36*, 77–93. [CrossRef]
12. Bajpai, P. *Recycling and Deinking of Recovered Paper*; Elsevier Science: Amsterdam, The Netherlands, 2013.

13. CANMET. *Pulp and Paper Sludge to Energy—Preliminary Assessment of Technologies, Canada*; CANMET Energy Technology Centre: Ottawa, ON, Canada, 2005.

14. Scott, G.M.; Smith, A. Sludge characteristics and disposal alternatives for the pulp and paper industry. In Proceedings of the 1995 International Environmental Conference, Atlanta, GA, USA, 7–10 May 1995; pp. 269–279.

15. Reza, M.T. *Upgrading Biomass by Hydrothermal and Chemical Conditioning*; University of Nevada Reno: Reno, NV, USA, 2013.

16. Reza, M.T.; Andert, J.; Wirth, B.; Busch, D.; Pielert, J.; Lynam, J.G.; Mumme, J. Hydrothermal Carbonization of Biomass for Energy and Crop Production. *Appl. Bioenergy* **2014**, *1*, 11–29. [CrossRef]

17. Reza, M.T.; Coronella, C.; Holtman, K.M.; Franqui-Villanueva, D.; Poulson, S.R. Hydrothermal Carbonization of Autoclaved Municipal Solid Waste Pulp and Anaerobically Treated Pulp Digestate. *ACS Sustain Chem. Eng.* **2016**, *4*, 3649–3658. [CrossRef]

18. Reza, M.T.; Mumme, J.; Ebert, A. Characterization of Hydrochar Obtained from Hydrothermal Carbonization of Wheat Straw Digestate. *Biomass Convers. Biorefin.* **2015**. [CrossRef]

19. Kruse, A.; Dinjus, E. Hot compressed water as reaction medium and reactant: Properties and synthesis reactions. *J. Supercrit. Fluids* **2007**, *39*, 362–380. [CrossRef]

20. Bandura, A.V.; Lvov, S.N. The ionization constant of water over wide ranges of temperature and density. *J. Phys. Chem. Ref. Data* **2006**, *35*, 15–30. [CrossRef]

21. Reza, M.T.; Uddin, M.H.; Lynam, J.; Hoekman, S.K.; Coronella, C. Hydrothermal carbonization of loblolly pine: Reaction chemistry and water balance. *Biomass Convers. Biorefin.* **2014**, *4*, 311–321. [CrossRef]

22. Reza, M.T.; Rottler, E.; Herklotz, L.; Wirth, B. Hydrothermal carbonization (HTC) of wheat straw: Influence of feedwater pH prepared by acetic acid and potassium hydroxide. *Bioresour. Technol.* **2015**, *182*, 336–344. [CrossRef] [PubMed]

23. Reza, M.T.; Wirth, B.; Luder, U.; Werner, M. Behavior of selected hydrolyzed and dehydrated products during hydrothermal carbonization of biomass. *Bioresour. Technol.* **2014**, *169*, 352–361. [CrossRef] [PubMed]

24. Reza, M.T.; Yan, W.; Uddin, M.H.; Lynam, J.G.; Hoekman, S.K.; Coronella, C.J.; Vasquez, V.R. Reaction kinetics of hydrothermal carbonization of loblolly pine. *Bioresour. Technol.* **2013**, *139*, 161–169. [CrossRef] [PubMed]

25. Lynam, J.G.; Reza, M.T.; Yan, W.; Vásquez, V.R.; Coronella, C.J. Hydrothermal carbonization of various lignocellulosic biomass. *Biomass Convers. Biorefin.* **2015**, *5*, 173–181. [CrossRef]

26. Makela, M.; Benavente, V.; Fullana, A. Hydrothermal carbonization of lignocellulosic biomass: Effect of process conditions on hydrochar properties. *Appl. Energy* **2015**, *155*, 576–584. [CrossRef]

27. Reza, M.T.; Lynam, J.G.; Vasquez, V.R.; Coronella, C.J. Pelletization of Biochar from Hydrothermally Carbonized Wood. *Environ. Prog. Sustain. Energy* **2012**, *31*, 225–234. [CrossRef]

28. Reza, M.T.; Yang, X.; Coronella, C.J.; Lin, H.; Hathwaik, U.; Shintani, D.; Neupane, B.P.; Miller, G.C. Hydrothermal Carbonization (HTC) and Pelletization of Two Arid Land Plants Bagasse for Energy Densification. *ACS Sustain. Chem. Eng.* **2015**. [CrossRef]

29. Saha, N.; Saba, A.; Reza, M.T. Effect of hydrothermal carbonization temperature on pH, dissociation constants, and acidic functional groups on hydrochar from cellulose and wood. *J. Anal. Appl. Pyrolysis* **2019**, *137*, 138–145. [CrossRef]

30. Naisse, C.; Alexis, M.; Plante, A.F.; Wiedner, K.; Glaser, B.; Pozzi, A.; Carcaillet, C.; Criscuoli, I.; Rumpel, C. Can biochar and hydrochar stability be assessed with chemical methods? *Org. Geochem.* **2013**, *60*, 40–44. [CrossRef]

31. Wiedner, K.; Naisse, C.; Rumpel, C.; Pozzi, A.; Wieczorek, P.; Glaser, B. Chemical modification of biomass residues during hydrothermal carbonization—What makes the difference, temperature or feedstock? *Org. Geochem.* **2013**, *54*, 91–100. [CrossRef]

32. Wiedner, K.; Rumpel, C.; Steiner, C.; Pozzi, A.; Maas, R.; Glaser, B. Chemical evaluation of chars produced by thermochemical conversion (gasification, pyrolysis and hydrothermal carbonization) of agro-industrial biomass on a commercial scale. *Biomass Bioenergy* **2013**, *59*, 264–278. [CrossRef]

33. Ronix, A.; Pezoti, O.; Souza, L.S.; Souza, I.P.A.F.; Bedin, K.C.; Souza, P.S.C.; Silva, T.L.; Melo, S.A.R.; Cazetta, A.L.; Almeida, V.C. Hydrothermal carbonization of coffee husk: Optimization of experimental parameters and adsorption of methylene blue dye. *J. Environ. Chem. Eng.* **2017**, *5*, 4841–4849. [CrossRef]

34. Kannan, S.; Gariepy, Y.; Vijaya Raghavan, G.S. Optimization of the conventional hydrothermal carbonization to produce hydrochar from fish waste. *Biomass Convers. Biorefin.* **2018**, *8*, 563–576. [CrossRef]

35. Kruse, A.; Zevaco, A.T. Properties of Hydrochar as Function of Feedstock, Reaction Conditions and Post-Treatment. *Energies* **2018**, *11*, 674. [CrossRef]

36. Román, S.; Libra, J.; Berge, N.; Sabio, E.; Ro, K.; Li, L.; Ledesma, B.; Álvarez, A.; Bae, S. Hydrothermal Carbonization: Modeling, Final Properties Design and Applications: A Review. *Energies* **2018**, *11*, 216. [CrossRef]

37. Kempegowda, R.S.; Skreiberg, Ø.; Tran, K.-Q.; Selvam, P.V.P. Techno-economic Assessment of Thermal Co-pretreatment and Co-digestion of Food Wastes and Sewage Sludge for Heat, Power and Biochar Production. *Energy Procedia* **2017**, *105*, 1737–1742. [CrossRef]

38. Escala, M.; Zumbuhl, T.; Koller, C.; Junge, R.; Krebs, R. Hydrothermal Carbonization as an Energy-Efficient Alternative to Established Drying Technologies for Sewage Sludge: A Feasibility Study on a Laboratory Scale. *Energy Fuel* **2013**, *27*, 454–460. [CrossRef]

39. Lucian, M.; Fiori, L. Hydrothermal Carbonization of Waste Biomass: Process Design, Modeling, Energy Efficiency and Cost Analysis. *Energies* **2017**, *10*, 211. [CrossRef]

40. Areeprasert, C.; Coppola, A.; Urciuolo, M.; Chirone, R.; Yoshikawa, K.; Scala, F. The effect of hydrothermal treatment on attrition during the fluidized bed combustion of paper sludge. *Fuel Process. Technol.* **2015**, *140*, 57–66. [CrossRef]

41. Areeprasert, C.; Zhao, P.T.; Ma, D.C.; Shen, Y.F.; Yoshikawa, K. Alternative Solid Fuel Production from Paper Sludge Employing Hydrothermal Treatment. *Energy Fuel* **2014**, *28*, 1198–1206. [CrossRef]

42. Zhao, P.T.; Ge, S.F.; Ma, D.C.; Areeprasert, C.; Yoshikawa, K. Effect of Hydrothermal Pretreatment on Convective Drying Characteristics of Paper Sludge. *ACS Sustain. Chem. Eng.* **2014**, *2*, 665–671. [CrossRef]

43. Areeprasert, C.; Ma, D.; Prayoga, P.; Yoshikawa, K. A Review on Pilot-Scale Applications of Hydrothermal Treatment for Upgrading Waste Materials. *Int. J. Environ. Sci. Dev.* **2016**, *7*, 425–430. [CrossRef]

44. Areeprasert, C.; Scala, F.; Coppola, A.; Urciuolo, M.; Chirone, R.; Chanyavanich, P.; Yoshikawa, K. Fluidized bed co-combustion of hydrothermally treated paper sludge with two coals of different rank. *Fuel Process Technol.* **2016**, *144*, 230–238. [CrossRef]

45. Mäkelä, M.; Forsberg, J.; Söderberg, C.; Larsson, S.H.; Dahl, O. Process water properties from hydrothermal carbonization of chemical sludge from a pulp and board mill. *Bioresour. Technol.* **2018**, *263*, 654–659. [CrossRef] [PubMed]

46. Makela, M.; Benavente, V.; Fullana, A. Hydrothermal carbonization of industrial mixed sludge from a pulp and paper mill. *Bioresour. Technol.* **2016**, *200*, 444–450. [CrossRef] [PubMed]

47. TAPPI. *Acid-Insoluble Lignin in Wood and Pulp*; (Reaffirmation of T 222 om-02); TAPPI: Peachtree Corners, GA, USA, 2006; Available online: https://www.tappi.org/content/SARG/T222.pdf (accessed on 4 March 2019).

48. Sequeira, R.M.; Lew, R.B. Carbohydrate composition of almond hulls. *J. Agric. Food Chem.* **1970**, *18*, 950–951. [PubMed]

49. Rong, H.; Wang, T.; Zhou, M.; Wang, H.; Hou, H.; Xue, Y. Combustion Characteristics and Slagging during Co-Combustion of Rice Husk and Sewage Sludge Blends. *Energies* **2017**, *10*, 438. [CrossRef]

50. Vamvuka, D.; El Chatib, N.; Sfakiotakis, S. Measurements of ignition point and combustion characteristics of biomass fuels and their blends with lignite. *Combustion* **2011**, *2015*, 95.

51. Funke, A.; Ziegler, F. Hydrothermal carbonization of biomass: A summary and discussion of chemical mechanisms for process engineering. *Biofuels Bioprod. Biorefin.* **2010**, *4*, 160–177. [CrossRef]

52. Hoekman, S.K.; Broch, A.; Robbins, C. Hydrothermal Carbonization (HTC) of Lignocellulosic Biomass. *Energy Fuel* **2011**, *25*, 1802–1810. [CrossRef]

53. Sheng, C.; Azevedo, J.L.T. Estimating the higher heating value of biomass fuels from basic analysis data. *Biomass Bioenergy* **2005**, *28*, 499–507. [CrossRef]

54. Zhao, C.; Jiang, E.; Chen, A. Volatile production from pyrolysis of cellulose, hemicellulose and lignin. *J. Energy Inst.* **2017**, *90*, 902–913. [CrossRef]

55. Kang, S.; Li, X.; Fan, J.; Chang, J. Characterization of Hydrochars Produced by Hydrothermal Carbonization of Lignin, Cellulose, d-Xylose, and Wood Meal. *Ind. Eng. Chem. Res.* **2012**, *51*, 9023–9031. [CrossRef]

56. Lin, Y.; Ma, X.; Peng, X.; Hu, S.; Yu, Z.; Fang, S. Effect of hydrothermal carbonization temperature on combustion behavior of hydrochar fuel from paper sludge. *Appl. Therm. Eng.* **2015**, *91*, 574–582. [CrossRef]

57. Kim, J.S.; Lee, Y.Y.; Park, S.C. Pretreatment of Wastepaper and Pulp Mill Sludge by Aqueous Ammonia and Hydrogen Peroxide. In *Twenty-First Symposium on Biotechnology for Fuels and Chemicals, Proceedings of the Twenty-First Symposium on Biotechnology for Fuels and Chemicals, Fort Collins, CO, USA, 2–6 May 1999*; Finkelstein, M., Davison, B.H., Eds.; Humana Press: Totowa, NJ, USA, 2000; pp. 129–139. [CrossRef]

58. Saba, A.; Saha, P.; Reza, M.T. Co-Hydrothermal Carbonization of coal-biomass blend: Influence of temperature on solid fuel properties. *Fuel Process. Technol.* **2017**, *167*, 711–720. [CrossRef]

59. García, G.; Arauzo, J.; Gonzalo, A.; Sánchez, J.L.; Ábrego, J. Influence of feedstock composition in fluidised bed co-gasification of mixtures of lignite, bituminous coal and sewage sludge. *Chem. Eng. J.* **2013**, *222*, 345–352. [CrossRef]

60. Grénman, H.; Eränen, K.; Krogell, J.; Willför, S.; Salmi, T.; Murzin, D.Y. Kinetics of Aqueous Extraction of Hemicelluloses from Spruce in an Intensified Reactor System. *Ind. Eng. Chem. Res.* **2011**, *50*, 3818–3828. [CrossRef]

61. McGaughy, K.; Reza, M.T. Recovery of Macro and Micro-Nutrients by Hydrothermal Carbonization of Septage. *J. Agric. Food Chem.* **2018**, *66*, 1854–1862. [CrossRef] [PubMed]

62. Wang, T.; Zhai, Y.; Zhu, Y.; Li, C.; Zeng, G. A review of the hydrothermal carbonization of biomass waste for hydrochar formation: Process conditions, fundamentals, and physicochemical properties. *Renew. Sustain. Energy Rev.* **2018**, *90*, 223–247. [CrossRef]

63. McKendry, P. Energy production from biomass (part 1): Overview of biomass. *Bioresour. Technol.* **2002**, *83*, 37–46. [CrossRef]

64. Stricker, G.D.; Flores, R.M.; Trippi, M.H.; Ellis, M.S.; Olson, C.M.; Sullivan, J.E.; Takahashi, K.I. *Coal Quality and Major, Minor, and Trace Elements in the Powder River, Green River, and Williston basins, Wyoming and North Dakota: U.S. Geological Survey*; U.S. Department of the Interior: Reston, VA, USA, 2007.

65. El-Sayed, S.A.; Mostafa, M. Pyrolysis characteristics and kinetic parameters determination of biomass fuel powders by differential thermal gravimetric analysis (TGA/DTG). *Energy Convers. Manag.* **2014**, *85*, 165–172. [CrossRef]

66. Yanfen, L.; Xiaoqian, M. Thermogravimetric analysis of the co-combustion of coal and paper mill sludge. *Appl. Energy* **2010**, *87*, 3526–3532. [CrossRef]

67. Volpe, M.; Goldfarb, J.L.; Fiori, L. Hydrothermal carbonization of Opuntia ficus-indica cladodes: Role of process parameters on hydrochar properties. *Bioresour. Technol.* **2018**, *247*, 310–318. [CrossRef] [PubMed]

68. Gao, Y.; Wang, X.; Wang, J.; Li, X.; Cheng, J.; Yang, H.; Chen, H. Effect of residence time on chemical and structural properties of hydrochar obtained by hydrothermal carbonization of water hyacinth. *Energy* **2013**, *58*, 376–383. [CrossRef]

69. He, C.; Giannis, A.; Wang, J.-Y. Conversion of sewage sludge to clean solid fuel using hydrothermal carbonization: Hydrochar fuel characteristics and combustion behavior. *Appl. Energy* **2013**, *111*, 257–266. [CrossRef]

70. Varol, M.; Atimtay, A.; Bay, B.; Olgun, H. Investigation of co-combustion characteristics of low quality lignite coals and biomass with thermogravimetric analysis. *Thermochim. Acta* **2010**, *510*, 195–201. [CrossRef]